

Design and Characterization of CMOS On-Chip Antennas for 60 GHz Communications

Diane TITZ^{1,2}, Fahd BEN ABDELJELIL¹, Sébastien JAN³, Fabien FERRERO^{1,2}, Cyril LUXEY^{2,4,5}, Patrice BRACHAT², Gilles JACQUEMOD^{1,2}

¹ Laboratoire d'Electronique, Antennes et Télécommunications, CNRS UMR6071, Université de Nice-Sophia-Antipolis, 250 rue A. Einstein, 06560 Valbonne, France

² CREMANT, University of Nice-Sophia-Antipolis, CNRS, France, Telecom Orange Labs

³ ST Microelectronics SA, T R&D, 850 rue Jean Monnet, 38926 Cedex Crolles, France

⁴ Institut Universitaire de France, 103 Boulevard Saint-Michel, 75005 Paris, France

⁵ Université de Nice Sophia Antipolis, IM2NP, UMR CNRS 6242, Sophia-Antipolis, France

diane.titz@unice.fr, cyril.luxey@unice.fr

Abstract. *In this paper, we present the design and the measurement of two antennas realized on a 130nm CMOS process. They both radiate in the 60 GHz band and are dedicated to Wireless Personal Area Network (WPAN) applications. The antennas are manufactured within the frame of a multi-wafer project with several surrounding microelectronic circuits. The first antenna is an Inverted-F antenna (IFA). It has a maximum gain of -8 dBi and a -10 dB matching bandwidth of 20%. The second radiator is a meandered dipole. It has a maximum gain of -14 dBi and a -10 dB matching bandwidth of 10%. The challenging measurement of their reflection coefficient and their gain radiation pattern are presented. Simulated versus measured curves are analyzed. We especially demonstrate the necessity to take into account the closest microelectronic circuits of the antennas for accurate modeling of the radiating performance of 60 GHz on-chip dies.*

Keywords

60 GHz communications, On-Chip antennas, Mm-wave radiation pattern set-up.

1. Introduction

The worldwide unlicensed band at 60 GHz offers new potentials for Wireless Personal Area Network (WPAN) applications [1]. Indeed, the 7 GHz available bandwidth is one hundred times wider than the one used in the 2.4 and 5 GHz Wi-Fi standards for personal communications. Thanks to this huge bandwidth, a new step in terms of transmission speed is now reachable. Therefore, around the world, several 60 GHz standards have been issued [2-4]. As the inherent oxygen absorption induces a strong attenuation of the electromagnetic waves around this frequency band, several possible communication scenarios have been studied. In [2-4], 1 to 10 meters Line-of-Sight

(LoS) and non-Line-of-Sight (nLoS) communications are examined. In terms of antenna-gain requirements, array-antennas with high-directivity seem to be the only solution to outcome the free space loss and the oxygen absorption. In addition, the nLoS communication cases require beam-forming and associated electronics. Therefore, designing such 60 GHz antennas is very challenging. Two different solutions exist. The first one is the Antenna-on-Chip (AoC) technology where the antenna is directly integrated with the front-end circuit on the same chip [5-6]. At millimeter-wave frequencies, this solution becomes more affordable thanks to the short wavelength of the electromagnetic waves. Moreover, silicon substrates have a high relative permittivity constant (usually $\epsilon_r = 11.9$) which also contributes to reduce the occupied size by the antennas. In addition, using bulk silicon technology process helps in reducing manufacturing costs. The second technique is the Antenna-in-Package (AiP) solution: the antenna is fabricated on a separate substrate and/or package and then integrated with the front-end circuit. This is the most common low-frequency solution as the antennas can be realized on cheaper and low-loss substrate and/or package. Consequently, several AiP integrations have been demonstrated at 60 GHz [7-9] as high gain and high total efficiency are easier to achieve at the expense of higher complexity and losses in the interconnections with the front-end module (usually done with wire bonding).

In this paper, we propose to investigate two different types of antennas realized on a 130nm CMOS process for 60 GHz WPAN communications. These antennas have been previously described in [10-11]. However, in [10], no measurement data were given and in [11], only the measurement of the reflection coefficient of one of the antenna was presented. In this paper, all the aforementioned measurements are given and deeply analyzed. An Inverted-F Antenna (IFA) is first designed on a 130nm-CMOS bulk process. The design methodology, simulations and new measurements are presented. In a second step, a meandered dipole is designed and characterized. The Ansys HFSS,

FEM-based-3D full wave solver is used for all the electromagnetic simulations. Simulated versus measured curves are analyzed and investigations to explain discrepancies are conducted. We especially demonstrate the necessity to take into account the closest microelectronic circuits of the antennas for accurate modeling of the radiating performance of 60 GHz on-chip dies. Finally, we also provide advices and guidelines for the radiation pattern measurement of 60 GHz on-chip antennas.

2. CMOS Process

Both antennas were realized on a 130nm CMOS process from ST Microelectronics. The CMOS process offers six possible metallization levels etched on a silicon substrate (Fig. 1).

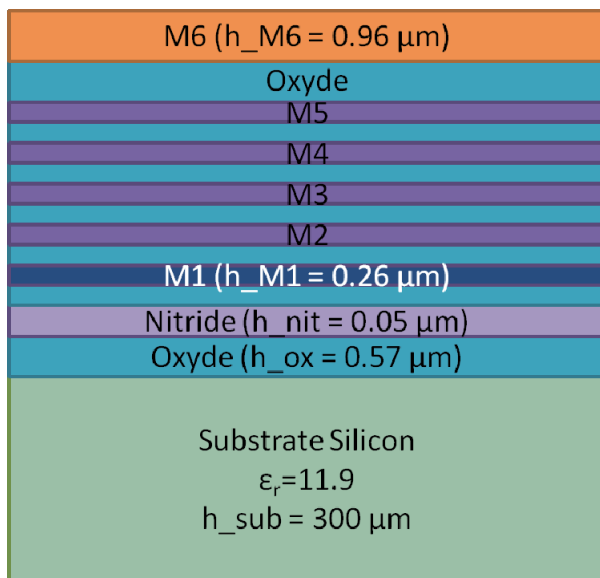


Fig. 1. Cross-sectionnal view of the different layers of the 130nm CMOS process from ST Microelectronics. The thickness of each layer is given in the drawing: thickness of M6 layer (h_{M6}), M1 layer (h_{M1}), Nitride layer (h_{nit}), Oxyde layer (h_{ox}) and Substrate layer (h_{sub}).

When designing CMOS antennas, an important practical consideration is to comply with the specific fabrication rules of the process: the metal density has to be kept between 20 and 80 % of the total area of the die. This is mandatory to avoid any mechanical failure of the fabricated die. We managed to avoid positioning those small metal parts in the vicinity of the open ends of the antennas to avoid strong disturbance of the electromagnetic field in those important regions [12]. It was done by creating exclusion areas in the layout. However, as explained before, these areas were chosen to be not too large in order to comply with the metal density rules of the process.

3. Inverted-F Antenna

3.1 Design of the Antenna

The IFA is a very popular planar antenna that has been used in a variety of applications [5]. It belongs to the class of the short-circuited monopoles. Basic design rules are given thereafter. The total length of the IFA, from the ground plane to its open end should be about a quarter of the guided wavelength at the operating frequency ($\lambda_g = 1.8$ mm here dealing with our 130nm process). Varying this length helps in tuning the resonance frequency of the IFA. The input impedance can be quite easily matched to 50Ω by modifying the spacing between the ground and the feeding strips. By increasing the height of the main arm of the IFA away from the ground plane, we can slightly decrease both the real part of its input impedance and its resonance frequency. Fig. 2 shows a top-view of the optimized 60-GHz IFA.

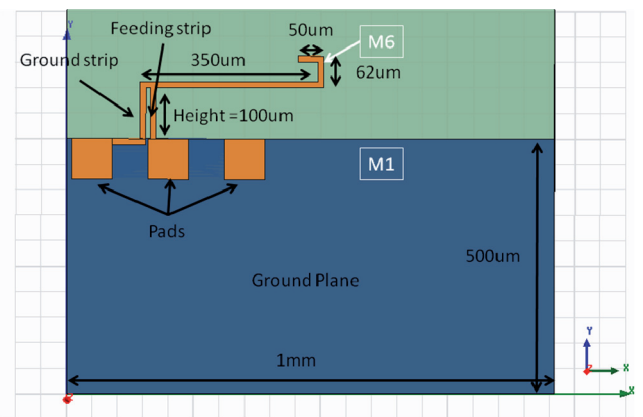


Fig. 2. Top-view of the optimized CMOS IFA.

The IFA is printed on the top metallization M6 and its ground plane on the lower metallization level M1 (see respectively orange and dark blue layers in Fig. 1 and 2). The antenna is fed via 150 μm -pitch Ground-Signal-Ground pads positioned on the M6 level. Each pad occupies an $80 \mu\text{m} \times 80 \mu\text{m}$ area. The capacitance effect of these pads, due to their position facing the ground plane has been taken into account in the optimization process of the input impedance of the antenna, so no further de-embedding technique is needed. The ground pads are connected to the lower metallization M1 using several vias, placed $0.22 \mu\text{m}$ away from each other and having a diameter of $0.19 \mu\text{m}$. The final AoC including the ground plane has a size of $0.7 \times 1 \text{ mm}^2$ ($0.39 \lambda_g \times 0.55 \lambda_g$). A top view of the layout of the optimized IFA is given in Fig. 3. It can be seen in this figure that the open end of the IFA was bended to achieve a top-loaded IFA structure. This additional capacitance effect helps to achieve a better 50Ω match and a wider -10dB matching bandwidth than the one of a straight IFA (see Fig. 4).

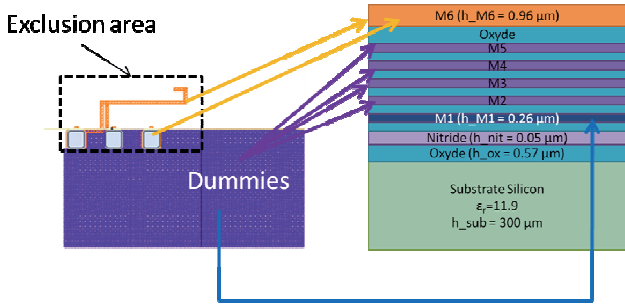


Fig. 3. Top view of the layout of the optimized CMOS IFA and corresponding layers of the 130nm CMOS process.

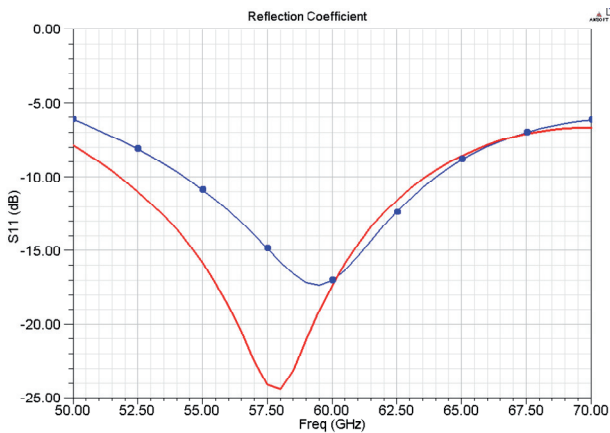


Fig. 4. Simulated reflection coefficient of the IFA. In red (thick line), the final IFA (top-loaded). In blue (circles), the straight IFA (without top-loading effect).

3.2 Simulation Results

A larger frequency-view of the simulated $|S_{11}|$ of the optimized IFA is presented in Fig. 5 (red curve). The frequency resonance, taken as the minimum of the $|S_{11}|$, occurs around 58 GHz. A -10 dB matching bandwidth of 20 % is obtained which easily covers the non-licensed 57-64 GHz band [1]. The simulated radiation efficiency was found to be 9 % which is comparable to the AoC designs described in [5], [6]. To understand the origin of such a low efficiency, we investigated the introduced losses of both the substrate and the metallization parts of the structure. First, we simulated the antenna with a fictitious ideal substrate with the same permittivity as the silicon ($\epsilon_r = 11.9$) but an infinite resistivity. Then, we simulated the IFA when setting the metallizations with infinite conductivity (PEC layer in HFSS). We found that the losses in the silicon substrate already represent 85 % of the total losses while metallization losses are only 15 % of these total losses. To check the validity of those simulations, we indeed verified that setting the IFA with a lossless substrate and lossless metallizations was resulting in a 100 % radiation efficiency.

Considering the size of the ground plane ($0.5 \times 1 \text{ mm}^2$ or $0.28 \lambda_g \times 0.55 \lambda_g$) and its possibility to strongly influence the radiating behavior of the structure, we also con-

ducted a parametric study. It was especially found that changing the size of the ground plane could slightly modify the frequency resonance but not the value of the radiation efficiency. Also, positioning this ground plane on either any metallization level of the CMOS substrate did not strongly change the value of the radiation efficiency.

3.3 Measurements

3.3.1 Reflection Coefficient

The measurement of the reflection coefficient was achieved at ST Microelectronics in Crolles. It was performed using on-wafer probing and a setup composed of one GSG Infinity probe and a 110 GHz Vector Network Analyzer (VNA). The whole chip including the IFA and the surrounding microelectronic circuits had to be glued onto a large wafer to cope with the measurement constraints of the test-bench and ensure its immobility regarding the metallic chuck. Therefore, we simulated this measurement configuration to take into account the influence of this larger wafer and the chuck. To simulate the conditions of this experiment, we modeled the large wafer and the chuck by one large box of Perfect Electric Conductor material (PEC). The width of this large box was determined from the results of several simulations: we demonstrated we could use the same dimensions as the radiation boundary box instead of the real dimensions of the wafer and the chuck and still obtain both a good accuracy and an acceptable simulation time. As shown in Fig. 5, a slightly different simulated reflection coefficient was obtained from this new simulation (green circles), especially a higher frequency resonance and a slightly worse impedance matching. However, with this new simulation, the simulation/measurement agreement was found to be remarkable for such a challenging measurement.

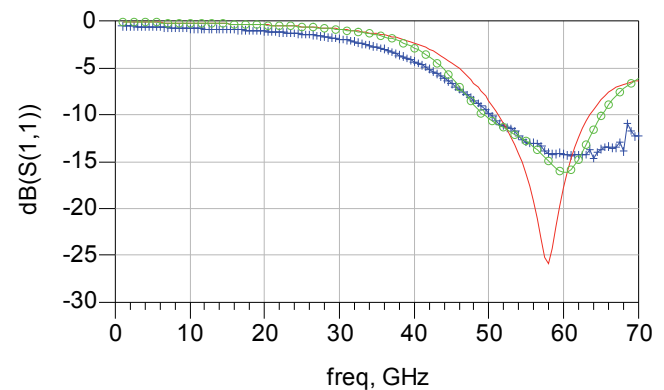


Fig. 5. Simulated (in light green circles) and measured (blue crosses) reflection coefficient of the IFA glued onto a larger wafer. Simulated reflection coefficient of the IFA (in red) without any large metallic wafer.

In a first attempt to be able to guess if the IFA was truly radiating and not acting as a dissipating matched load, we placed a metallic probe in front of the antenna, to disturb its electromagnetic near field. The measured input

impedance is presented on a Smith Chart in Fig. 6. It can be seen that the IFA clearly radiates because the dark blue curve of the input impedance of the IFA measured without any objects in its reactive near-field is strongly perturbed in comparison with the purple curve which represents the measurement of the input impedance of the disturbed IFA by the metallic probe.

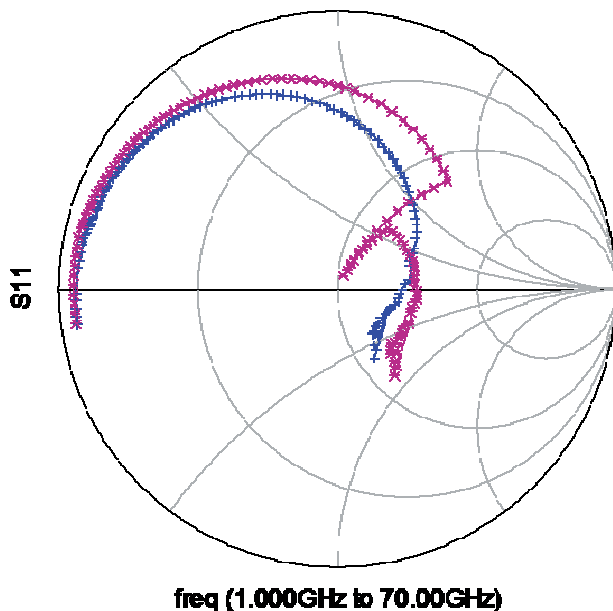


Fig. 6. Measured (dark blue crosses) S_{11} of the IFA. Purple stars when the metallic tip of another probe is closely placed in front of the IFA.

3.3.2 Measurements of the Radiation Pattern

The setup described in [11-13] was used to measure the 3D radiation pattern of the IFA. The probe-based 3D measurement setup is shown in Fig. 7. It uses a special plastic carrier and therefore the ability to leave free space from the close neighborhood of the antenna (no metallic chuck). The die is supported by a fixture in rigid foam, which provides the good support for the probe to touch GSG testing pad for measurements. Hence, using the two rotating arms (in grey in Fig. 7), the measurement of the 3D radiation pattern and the full E- and H-planes (either above or below the antenna) is possible. A PNA is feeding the antenna with a 60 GHz signal through the GSG probe. At the receive side, a mixer is directly connected to the horn antenna to down convert the signal to lower frequencies. Therefore, the two arms can rotate without degrading the quality of the measurement. Everything is fully automatic and controlled by computer. The measurement is then fast and reliable. The accuracy of the setup has been carefully computed from the measurement and/or the use of the manufacturer insertion loss data of all the elements of the RF chain: less than 1 dB.

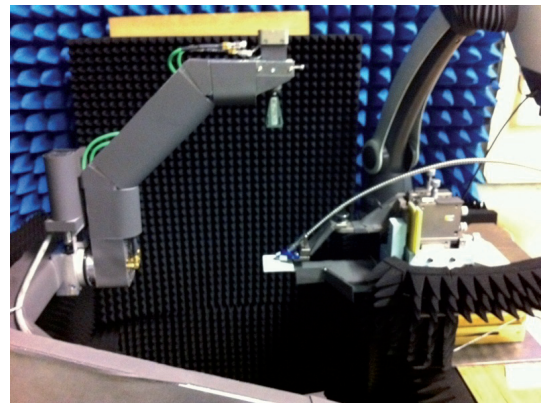


Fig. 7. Photograph of the probe-based 3D measurement setup.

As illustrated in Fig. 8a, the IFA and the dipole antenna were fabricated on the same die and they were surrounded by several RF microelectronic circuits (mixer, VCO, CMOS switches and LNA). In a more accurate simulation, we decided to take into account those surrounding circuits as plain metallic parts positioned on the M6 level. A top-view of the simulated IFA model surrounded by the whole die is shown in Fig. 8b. It was especially found that the influence of the surrounding elements was negligible on the reflection coefficient but not on the radiation patterns.

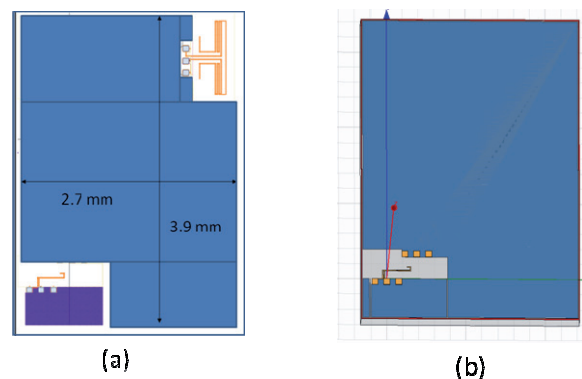


Fig. 8. Top-view of the (a) fabricated die with a clearance of the IFA (lower left-side corner) and the dipole antenna (upper right-side corner) and (b) simulated die of the IFA with HFSS.

The simulated radiation patterns of the IFA without the surrounding circuits (Fig. 2) and with them (Fig. 8b) are respectively presented in Fig. 9a and b. The novel radiation pattern is totally different from the previous one, therefore, including the total die in the simulation model seems to be very important. From almost a dipole-like radiation pattern in Fig. 9a, we have now a completely distorted pattern (Fig. 9b) with several maximums in different directions and also several nulls. The maximum total gain which occurs in completely different directions for the two structures is 2 dB higher when including the die in the simulation model. It is equal to -7.9 dBi in the ($\varphi = 90^\circ$,

$\theta = 98^\circ$) direction without the whole die and -5.9 dBi in the ($\varphi = 50^\circ, \theta = 134^\circ$) direction with it.

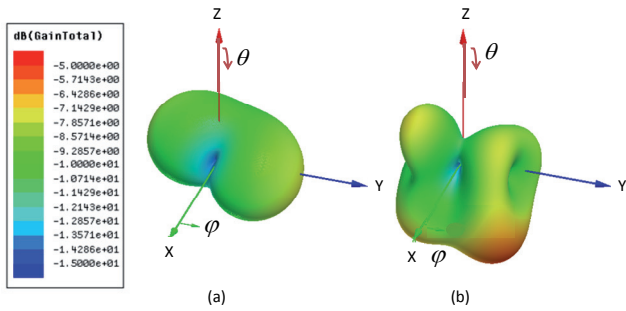


Fig. 9. Simulated radiation pattern of the IFA. In (a) the IFA from Fig. 2 is simulated, in (b) the IFA from Fig. 8b is simulated.

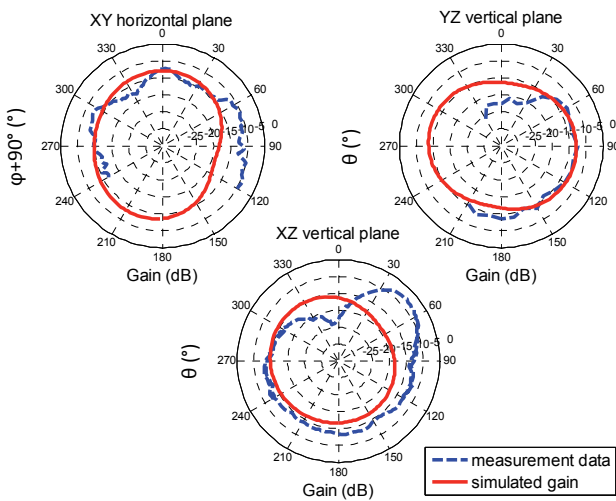


Fig. 10. Simulation and measurement of the gain radiation pattern in three main planes at 60 GHz. The IFA is simulated without the surrounding circuits.

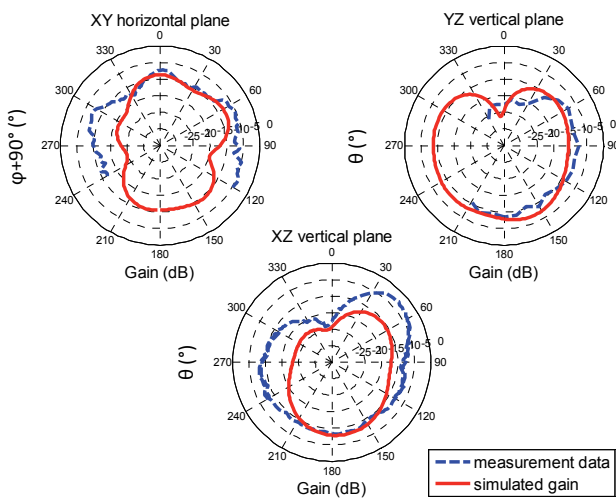


Fig. 11. Simulation and measurement of the gain radiation pattern in three different planes of the total die at 60 GHz. The IFA is simulated with the surrounding circuits.

Fig. 10 and 11 show the comparison between simulated and measured radiation patterns cuts of the IFA (three main planes), without the surroundings circuits (Fig. 10) and with the whole die (Fig. 11). Measurement over the whole plane is not always possible due to the probe positioner [11]. In Fig. 10, the probe is positioned at $\varphi = 180^\circ$ in the XY horizontal plane and at $\theta = 270^\circ$ in the YZ vertical plane that's why the measured curves are not complete in those planes. The first comment goes toward the shape of the measured radiation patterns versus the simulated ones. In Fig. 10, when the surrounding circuits are not taken into account, a poor agreement is observed with the measured values. However, a very good agreement is found between the curves in Fig. 11 which reinforce the necessity to take into account the surrounding parts of the IFA. However, the simulated and measured gain values are not in a perfect agreement, except in the YZ plane. The simulated and measured values of the maximum gain in each plane are given in Tab. 1. A ± 1 -dB accuracy has been computed during the calibration stage before the measurements. A better accuracy is difficult to obtain, especially at 60 GHz. Moreover, many other elements exist in the vicinity of the AUT like the antenna and the probe positioner holders. These elements are difficult to be accurately modeled without a dramatic increase of the simulation time. Also, the antenna is fed by a probe which is another source of radiation at 60 GHz. This additional radiator can perturb the radiation of the antenna itself, especially when its maximum gain is not really high.

Plane	XY horizontal	YZ vertical	XZ vertical
Measurement	-4.3dBi at $\varphi = 116^\circ$	-7.5dBi at $\theta = 100^\circ$	-2.7dBi at $\theta = 50^\circ$
Simulation without the die	-7.9dBi at $\varphi = 4^\circ$	-7.8dBi at $\theta = 102^\circ$	-9.5dBi at $\theta = 298^\circ$
Simulation with the total die	-8dBi at $\varphi = 59^\circ$	-7dBi at $\theta = 160^\circ$	-7.7dBi at $\theta = 172^\circ$

Tab. 1. Measured and simulated maximum gain values in each plane (with corresponding directions).

4. Dipole Antenna

4.1 Design of the Antenna

The length of each arm of a dipole is taken slightly less than a quarter of a guided wavelength at the operating frequency. One solution to reduce the occupied area consists in meandering the arms of the dipole at the expense of a decrease of the impedance bandwidth. Tuning the input impedance of a dipole to $(50+j0) \Omega$ can be done by changing the way you meander those arms and/or by inserting a crossbar between them [14]. This technique consists in reinforcing an inductance or a capacitance effect over the input impedance depending of the width and the position of the crossbar versus the arms of the dipole. The dipole optimized with this technique is presented in Fig. 12. The same feeding pads as the ones used for the IFA have been positioned to feed the dipole. Due to a limited allocated

area on the die, we could not design and include a dedicated balun to feed the dipole. However, the cross-bar technique helped us in solving this excitation problem. As can be noticed the length of each arm of the dipole is longer than $\lambda_g/4$ which would be equal to 450 μm on this Silicon substrate. This crossbar technique was not properly working on the $\lambda_g/4$ dipole, so we decided to use the dipole at its first higher-order mode at 60 GHz. The same CMOS process constraints as the ones described in part 2 were observed. The overall chip size is $0.6 \times 1 \text{ mm}^2$ ($0.33 \lambda_g \times 0.55 \lambda_g$).

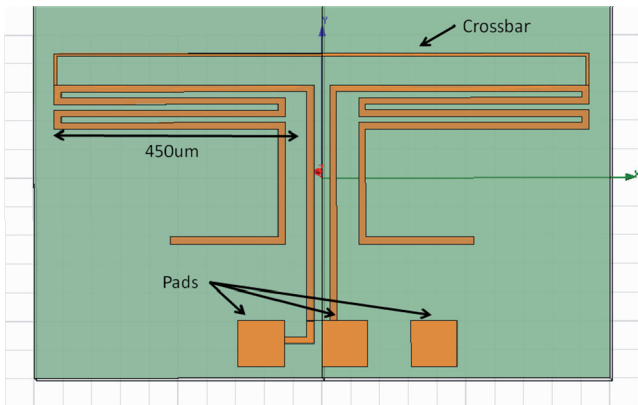


Fig. 12. Top-view of the optimized CMOS dipole antenna.

4.2 Simulation Results

The simulated $|S_{11}|$ of the dipole is presented in Fig. 13 (red curve). The frequency resonance of the structure, taken as the minimum of the $|S_{11}|$ occurs around 60.5 GHz. A -10 dB matching bandwidth of 10% was obtained. The simulated radiation efficiency was found to be 2 %. We also found that the silicon substrate was contributing to the total losses in a 85% proportion.

4.3 Measurements

4.3.1 Reflection Coefficient

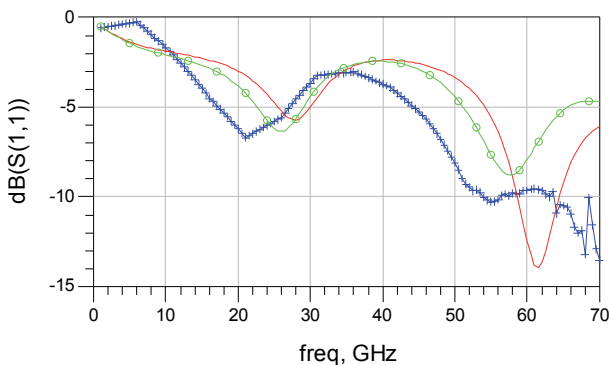


Fig. 13. Simulated (in light green circles) and measured (blue crosses) reflection coefficient of the IFA glued onto a larger wafer. Simulated reflection coefficient of the dipole (in red) without the large wafer.

The measurement of the reflection coefficient was also achieved at ST Microelectronics in Crolles (blue curve in Fig. 13). The dipole was again placed on a large wafer to cope with the measurement facility. We simulated this experimental condition. As shown in Fig. 13, taking into account the large wafer allows finding a better agreement between simulated and measured curves (blue and green) especially if we focus on the absolute value of the reflection coefficient.

4.3.2 Measurements of the Radiation Pattern

The setup described in [11-13] was used for the radiation pattern measurements. In Fig. 14, we can see the simulated radiation pattern of the dipole alone (Fig. 12) and the simulated radiation pattern including the total die like we did for the IFA (see Fig. 8a to see where the dipole is placed on the total die). Taking the total die into account for this dipole antenna seems to be even more important than the IFA case as the novel radiation pattern is totally different. From a dipole-like pattern with omnidirectional radiation in the YZ plane (Fig. 14a), we can see a completely different pattern (Fig. 14b) with maximum radiation in the orthogonal direction of the previous ones (+X and -X directions). When the whole die is taken into account, we obtain a null at $\varphi = 90^\circ$ (maximum gain in this direction in the simulation model without the whole die). The maximum gain absolute value is almost doubled when the dipole is surrounded by all the circuits. The maximum gain is equal to -14.3 dBi in the ($\varphi = 274^\circ, \theta = 10^\circ$) direction without the whole die and -7.9 dBi in the ($\varphi = 314^\circ, \theta = 134^\circ$) direction with it.

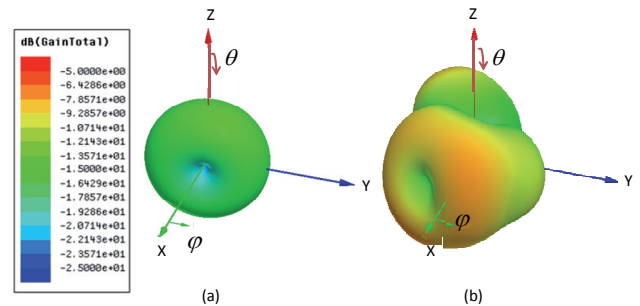


Fig. 14. Simulated radiation pattern of the dipole. In (a) the dipole from Fig. 12 is simulated (without die). In (b) the dipole from Fig. 8a is simulated (total die is taken into account).

Fig. 15 and 16 show the comparison between simulated and measured radiation patterns cuts of the dipole (three main planes), without the surroundings circuits (Fig. 15) and with the whole die (Fig. 16). In Fig. 15, when the surrounding circuits are not taken into account in the simulated patterns, a poor agreement is observed with the measured values. However, a very good agreement is found between the shapes of the measured radiation patterns versus the simulated ones with the whole die which reinforce the necessity to take into account the surrounding parts of the antenna at those frequencies. However, the

simulated and measured gain values are not in perfect agreement, except in the XY and XZ planes. The simulated and measured maximum gain values in each plane are given in Tab. 2. The accuracy of these values is given with ± 1 dB. There seems to be a better match between the absolute simulated and measured gain levels than the IFA case.

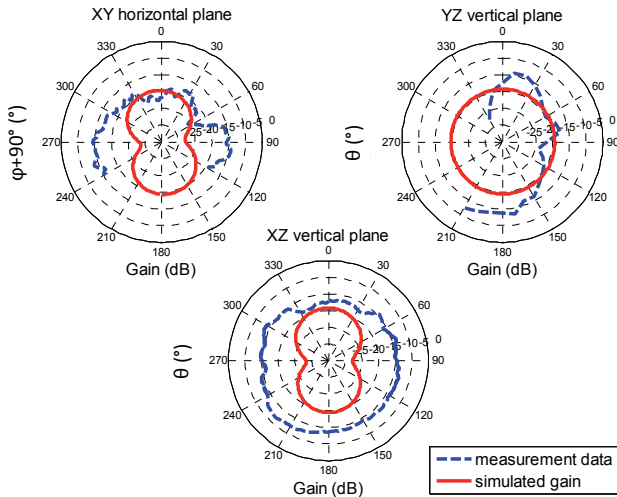


Fig. 15. Simulation and measurement of the gain radiation pattern in the three main planes at 60 GHz. The dipole is simulated without the surrounding circuits.

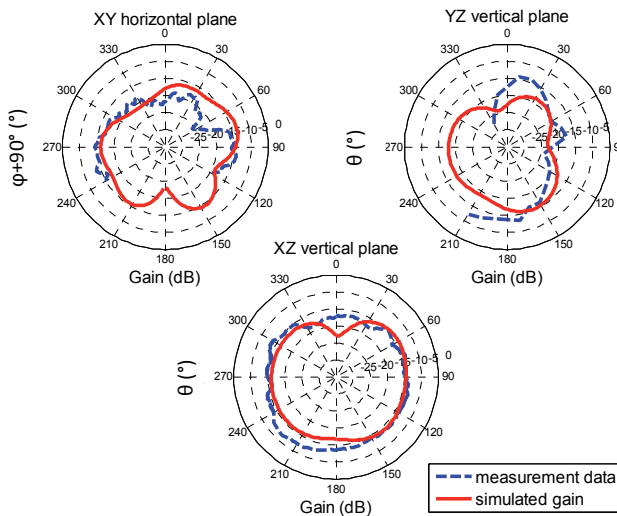


Fig. 16. Simulation and measurement of the gain radiation pattern in the three main planes at 60 GHz. The dipole is simulated with the surrounding circuits.

Plane	XY horizontal	YZ vertical	XZ vertical
Measurement	-8.7dBi at $\varphi=252^\circ$	-7.1dBi at $\theta=210^\circ$	-6.7dBi at $\theta=222^\circ$
Simulation without the die	-14.3dBi at $\varphi=172^\circ$	-14.3dBi at $\theta=354^\circ$	-14.3dBi at $\theta=0^\circ$
Simulation with the total die	-8.5dBi at $\varphi=74^\circ$	-10.3dBi at $\theta=152^\circ$	-8.9dBi at $\theta=124^\circ$

Tab. 2. Measured and simulated maximum gain values in each plane (with corresponding directions).

5. Conclusion

The aim of this paper was to investigate CMOS antennas operating at 60 GHz. We presented the design, the impedance and radiation pattern characterization of two antennas fabricated on a 130nm CMOS process. Our study has enlightened some very important facts. During the reflection coefficient and radiation pattern measurements, we noticed strong differences between simulated and measured data especially dealing with the radiation patterns. This led us to investigate what should be taken into account in the simulation model of 60 GHz on-chip antennas. It was especially found that all the surrounding metallic parts of the antennas have to be considered, however in a different manner either for the reflection coefficient or the radiation patterns. As antenna arrays with directive radiation are the only possible solution at 60 GHz for WPAN Non-Light-Of-Sight communications, their design should also be handled very cautiously. Indeed, the whole RF chip with the radio front-end module has to be included in the simulation model to avoid any deviation in the expected pointing direction of the radiation.

We also conducted a specific study to understand which losses are the most preeminent in those CMOS structures. It was demonstrated that the low resistivity of the substrate was mainly responsible for the poor radiation efficiency of our two different antennas. No superiority of the IFA over the dipole was demonstrated. More precisely, our results were found to be comparable to other antenna-concepts realized on identical CMOS substrate at 60 GHz but sometimes radiating in a different manner (directive Yagi in the horizontal plane) [15]. A possible improvement of the radiation efficiency could be achieved by using high-resistivity substrate or other Silicon process such as Silicon-on-Insulator (SOI).

Acknowledgements

The authors would like to thank the CIMPACA Design Platform, ST-Microelectronics and Orange Labs for their help, support and technical discussions.

References

- [1] SMULDERS, P. Exploring the 60 GHz band for local wireless multimedia access: Prospects and future direction. *IEEE Communication Magazine*, 2002, vol. 40, no. 1, p. 140 - 147.
- [2] IEEE 802.15 WPAN Task Groups 3c, IEEE Standard 802, 2005.
- [3] IEEE 802.11 Task Groups ad, IEEE Standard 802, 2009.
- [4] ECMA-387 Standard, 2008. Available: <http://www.ecma-international.org/publications/standards/Ecma-387.htm>

- [5] GUO, P.-J., CHUANG, H.R. A 60-GHz millimeter-wave CMOS RFIC-on-chip meander-line planar inverted-F antenna for WPAN applications. In *Proceedings of AP-S International Symposium*. San Diego (USA), 2008, p. 1 - 4.
- [6] ZHANG, Y. P., SUN, M., GUO, L. H. On-chip antennas for 60-GHz radios in silicon technology. *IEEE Transactions on Electronic Devices*, 2005, vol. 52, no. 7, p. 1664 - 1668.
- [7] SUN, M., ZHANG, Y. P., ONG, L. C., GUO, Y. X., KARIM, M.F. Integration of linearly- and circularly-polarized arrays in packages for 60 GHz radios in LTCC technology. In *Proceedings of European Conference on Antenna and Propagation*. Barcelona (Spain), 2010, p. 1 - 4.
- [8] ZHANG, Y. P., LIU, D. Antenna-on-chip and antenna-in-package solutions to highly integrated millimeter-wave devices for wireless communications. *IEEE Transactions on Antennas and Propagation*, 2009, vol. 57, no. 10, p. 2830 - 2841.
- [9] MARTINEZ-VASQUEZ, M., HOLZWARTH, S., OIKONOMOPOULOS-ZACHOS, C., RIVERA, A. Wideband, balanced-fed 60 GHz antennas for integrated transceivers on LTCC substrate. In *Proceedings of European Conference on Antenna and Propagation*. Barcelona (Spain), 2010, p. 1 - 4.
- [10] TITZ, D., BEN ABDELJELIL, F., LUXEY, C., JACQUEMOD, G. Co-design of integrated antennas and CMOS switches for future indoor personal networks at 60 GHz. In *Proceedings of AP-S International Symposium*. Toronto (Canada), 2010, p. 1 - 4.
- [11] TITZ, D., KYRÖ, M., LUXEY, C., BEN ABDELJELIL, F., JACQUEMOD, G., VAINIKAINEN, P. Radiation pattern measurement set-up for 60 GHz on-chip antennas. In *Proceedings of Loughborough Antennas and Propagation Conference*. Loughborough (UK), 2010, p. 533 - 536.
- [12] BARAKAT, M. H., NDAGIJIMANA, F., DELAVALD, C. On the design of 60 GHz integrated antennas on 0.13 μm SOI technology. In *Proceedings of International SOI Conference*. Indian Wells (USA), 2007, p. 117 - 118.
- [13] RANVIER, S., KYRÖ, M., ICHELN, C., LUXEY, C., STARAJ, R., VAINIKAINEN, P. Compact 3-D on-wafer radiation pattern measurement system for 60 GHz antennas. *Microwave and Optical Technology Letters*, 2009, vol. 51, no. , p. 319 - 324.
- [14] BALANIS, C. A. *Antenna Theory: Analysis and Design*. 3rd ed. New York: John Wiley & Sons, 2005.
- [15] HSU, S.-S., WEI, K.-C., HSU, C.-Y., CHUANG, H. R. A 60-GHz millimeter-wave CPW-fed Yagi antenna fabricated by using 0.18- μm CMOS technology. *IEEE Electron Device Letters*, 2008, vol. 29, no. 6, p. 625 - 627.

About Authors

Diane TITZ was born in Paris, France, in 1985. She received her M.Sc. with honors from the University of Paris-Sud (XI) and the ENS de Cachan in 2009. She is currently working towards her PhD at the LEAT-CNRS (Laboratoire d'Electronique Antennes et Télécommunications) from the University of Nice-Sophia Antipolis, France and the CREMANT (Centre de Recherche Mutualisé sur les Antennes), joint lab between the University of Nice-Sophia Antipolis and Orange Labs. Her research interests include 60 GHz communications especially in the field of antenna design, measurements, and passive circuits. She has authored or co-authored 11 publications in international and European conferences.

Fahd BEN ABDELJELIL was born in Nice, France, in 1983. He received his M.Sc. degree in electrical engineering from Polytechnic School of the University of Nice Sophia-Antipolis in 2006 and his Ph.D. degree in electrical engineering from the University of Nice-Sophia Antipolis in 2010. His research interests are in the field of RF design and high-frequency integrated circuits for telecommunications.

Sébastien JAN is an engineer in ST-Microelectronics Crolles.

Fabien FERRERO was born in Nice, France, in 1980. He received his engineer degree and his M.Sc. degree in electrical engineering from Polytechnic School of the University of Nice Sophia-Antipolis and the University of Nice-Sophia Antipolis in 2003. He received his Ph.D. degree in electrical engineering in 2007 from the University of Nice-Sophia Antipolis. From 2008 to 2009, he worked for IMRA Europe (Aisin Seiki research center) as a research engineer and developed automotive antennas. He is currently an Associate Professor at the Polytechnic school of the University of Nice Sophia-Antipolis. He is doing his research at the LEAT (Laboratoire d'Electronique, Antennes et Télécommunications). His studies concerned design and measurement of millimetric antennas, phase shifters and reconfigurable antennas.

Cyril LUXEY was born in Nice, France in 1971. He received the Ph.D. degree in electrical engineering (1999), with honors, from the University of Nice-Sophia Antipolis, France. Since 2009, he is a Full Professor at the IUT Réseaux et Télécoms in Sophia-Antipolis where he is the head of a technical bachelor degree and where he teaches electromagnetic and electronics. In October 2010, he has been appointed as a Junior Member of the "Institut Universitaire de France (IUF)" institution for five years. He holds an Institut Universitaire de France chair, selectively awarded to faculty professors in France for research excellence. His current research interests include the design and measurement of electrically small antennas, multi-antenna systems, diversity and MIMO techniques, RFID antennas, silicon-based active integrated and MEMS-based printed antennas, antennas for biomedical applications and antennas for LTCC modules at 60 and 120 GHz. He is an IEEE Senior Member, a reviewer for several IEEE and IET journals and conferences. Cyril Luxey and his students received the H.W. Wheeler Award of the IEEE Antennas and Propagation Society for the best application paper of the year 2006. Cyril Luxey has authored or co-authored more than 180 papers. He will be the general chair of the Loughborough Antennas and Propagation Conference in 2011.

Patrice BRACHAT received the telecommunication and electrical degree from Ecole Nationale Supérieure des Télécoms (ENST), Paris, in 1978, the Ph.D. degree in 1980 and the HdR degree from Université de Nice Sophia Antipolis in 1998. In 1992 he was in charge of the Antenna

Research Group in the La Turbie Orange Lab. Since 1992 he also holds scientific appointments at university of Nice Sophia Antipolis (France). Since 2008 he is co-head of the CREMANT, the antenna joint research center between the Orange Labs, the Nice University and the CNRS. His professional interests include the areas of antenna design, small antennas and computational electromagnetics. Since 2000 he was vice chairman of the JINA conference in NICE. In 2006 he was local chairman of the successful EuCAP06 conference in Nice. Since 2006 he is Senior Member IEEE.

Gilles JACQUEMOD received his M.Sc. Degree in Microelectronics Engineering from ICPI Lyon, and the M. Sc. Degree (DEA) from Centrale Lyon, France in 1986, and the Ph.D Degree from INSA Lyon in 1989. From 1990 to 2000, he worked at LEOM, Ecole Centrale Lyon, as an Associate Professor. In 2000, he joined the LEAT laboratory and the Ecole Polytechnique of Nice – Sophia Antipolis University as full professor. His primary research interests include analog and integrated circuit design and behavioral modeling of mixed domain systems. He is also involved in RF design applied to wireless communications.